

Hard-Core Bosons on the Kagome Lattice: Valence-Bond Solids and Their Quantum Melting

S. V. Isakov,¹ S. Wessel,² R. G. Melko,³ K. Sengupta,⁴ and Yong Baek Kim¹

¹*Department of Physics, University of Toronto, Toronto, Ontario M5S 1A7, Canada*

²*Institut für Theoretische Physik III, Universität Stuttgart, 70550 Stuttgart, Germany*

³*Materials Science and Technology Division, Oak Ridge National Laboratory, Oak Ridge, Tennessee 37831, USA*

⁴*TCMP Division, Saha Institute of Nuclear Physics, 1/AF Bidhannagar, Kolkata-700064, India*

(Received 22 February 2006; published 6 October 2006)

Using large scale quantum Monte Carlo simulations and dual vortex theory, we analyze the ground state phase diagram of hard-core bosons on the kagome lattice with nearest-neighbor repulsion. In contrast with the case of a triangular lattice, no supersolid emerges for strong interactions. While a uniform superfluid prevails at half filling, two novel solid phases emerge at densities $\rho = 1/3$ and $\rho = 2/3$. These solids exhibit an only partial ordering of the bosonic density, allowing for local resonances on a subset of hexagons of the kagome lattice. We provide evidence for a weakly first-order phase transition at the quantum melting point between these solid phases and the superfluid.

DOI: 10.1103/PhysRevLett.97.147202

PACS numbers: 75.10.Jm, 05.30.Jp, 67.90.+z, 75.40.Mg

Current interest in microscopic models of frustrated quantum systems stems largely from the search for exotic quantum phases and spin liquid states. In general, geometric frustration tends to destabilize quasiclassical order, possibly allowing for nontrivial quantum states and novel critical phenomena to emerge in such systems. One intriguing approach addresses classically frustrated (Ising) models perturbed by quantum (off-diagonal) interactions [1]. The behavior of classically disordered, degenerate ground state manifolds upon application of a U(1) symmetric perturbation (e.g., ferromagnetic exchange) is of special interest, as experimental advances in the construction and control of atomic gases in optical lattices have opened up the possibility of designing such Hamiltonians for ultracold bosons. In particular, it has recently been shown how an optical kagome lattice can be constructed using a triple laser beam design [2], which could permit access to parameter regions of interest in the search for exotic quantum phenomena.

In this Letter, we consider a model of bosons on the kagome lattice in the strongly interacting regime, corresponding to the hard-core limit of the Bose-Hubbard Hamiltonian discussed in Ref. [2],

$$H_b = -t \sum_{\langle i,j \rangle} (b_i^\dagger b_j + \text{H.c.}) + V \sum_{\langle i,j \rangle} n_i n_j - \mu \sum_i n_i, \quad (1)$$

where b_i^\dagger (b_i) creates (destroys) a particle on site i , $t > 0$ denotes the nearest-neighbor hopping, $V > 0$ is the nearest-neighbor repulsion, and μ is the chemical potential. This model can also be mapped onto the spin-1/2 XXZ model [3], allowing for an interpretation of our results in terms of both bosons and quantum spins. We report results on the ground state phase diagram obtained from a combined analysis of large scale quantum Monte Carlo (QMC) simulations using the stochastic series expansion technique [4,5] and phenomenological dual vortex theory (DVT) [6,7]. We find that, in contrast to previous theoretical

expectations, a uniform superfluid persists at half filling for all values of V/t . In addition, for fillings $\rho = 1/3$ and $2/3$, we find evidence for valence-bond solid (VBS) phases where bosons are delocalized around a subset of hexagons (see Fig. 1). We find that the quantum melting of both VBS phases into the superfluid occurs at weakly first-order quantum phase transitions.

Past work on the ground state phase diagram of this model has been controversial and intriguing: Spin-wave calculations suggest that a supersolid state may emerge around half filling ($\rho = 1/2$) at $\mu = 2V$ for $t/V < 0.5$ [8]. However, these results are not conclusive, since strong quantum fluctuations may destroy the long-range order assumed within mean-field theory [8]. More recently, consideration of the large classical degeneracy [9] at $t = 0$ has led to the proposal of several exotic Mott-insulating states (e.g., VBSs or disordered quantum liquids) at half filling

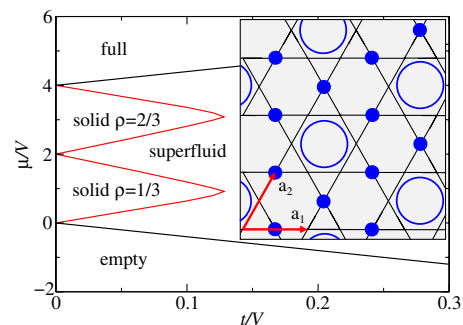


FIG. 1 (color online). Ground state phase diagram of hard-core bosons on the kagome lattice (inset). The primitive vectors \mathbf{a}_1 and \mathbf{a}_2 are constrained on a (periodic) torus spanned by $\mathbf{L}_1 = n_1 \times \mathbf{a}_1$ and $\mathbf{L}_2 = n_2 \times \mathbf{a}_2$ (where $a_1 = a_2 = 2$). The circles illustrate the subset of hexagons with a resonating boson occupation of three bosons per hexagon in the $\rho = 2/3$ solid. The remaining bosons localize to form a solid backbone on the sites that do not belong to any of these hexagons.

[10]. Very little work has been done to elucidate the nature of the phase diagram away from half filling.

Using QMC simulations, we have obtained the phase diagram of H_b , illustrated in Fig. 1. The lattice is empty for $\mu \leq -4t$ and completely filled for $\mu \geq 4(t+V)$. For large values of t/V , the bosons are superfluid, with a finite value of the superfluid density ρ_s , which we measure through winding number fluctuations $W_{a_{1,2}}$ [11] in each of the lattice directions as $\rho_s = (\langle W_{a_1}^2 \rangle + \langle W_{a_2}^2 \rangle) / (2\beta t)$, where β is the inverse temperature. In agreement with mean-field theory, we find that two solid phases with rational fillings $\rho = 1/3$ and $2/3$ emerge at smaller t/V . Both are characterized by finite values (in the thermodynamic limit) of the density structure factor per site $S(\mathbf{q})/N = \langle \rho_{\mathbf{q}\tau} \rho_{\mathbf{q}\tau}^\dagger \rangle$ and the static susceptibility per site $\chi(\mathbf{q})/N = \langle \int d\tau \rho_{\mathbf{q}\tau} \rho_{\mathbf{q}0}^\dagger \rangle$, where $\rho_{\mathbf{q}\tau} = (1/N) \sum_i \rho_{i\tau} \exp(i\mathbf{q}\mathbf{r}_i)$ and $\rho_{i\tau}$ is the boson density at site i and imaginary time τ , at wave vectors $\mathbf{q} = \mathbf{Q} \equiv (2\pi/3, 0)$. This can be seen in Fig. 2, which shows peaks at the corners of the Brillouin zone (BZ) in the solid phase that are absent in the superfluid.

Decreasing t/V at half filling ($\mu/V = 2$), the value of ρ_s in the limit $V \rightarrow \infty$ ($t = 1$) takes on about 54% of its value at the XY point, $\rho_s(V = 0) \approx 0.55$ (see Fig. 3). This is in stark contrast to the triangular lattice case, where $\rho_s(V \rightarrow \infty)$ approaches only about 4% of its value at the XY point [12]. We do not observe evidence of long-range order in the density structure factor, thus eliminating the possibility of a supersolid phase as found recently on the triangular lattice at small values of t/V [12–14]. In addition, we do not observe any Bragg peaks in the bond-bond structure factor (defined below), precluding the existence of any VBS order. The persistence of the superfluid phase can be understood from a duality analysis of the boson problem in terms of vortices on the dual dice lattice, which interact with a dual magnetic flux of $2\pi p/q = \pi$ (for boson filling $\rho = p/q = 1/2$) [6,7]. It has been shown that for the dice lattice at $\rho = 1/2$ the vortices undergo dynamic localization due to an Aharonov-Bohm caging effect [15] that

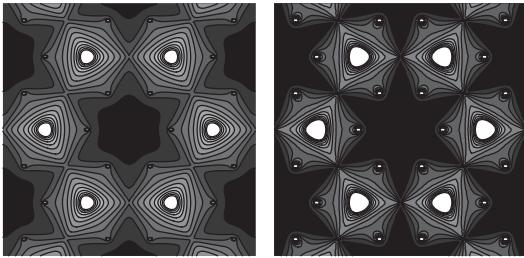


FIG. 2. Contour plots of the structure factor (left panel) and the static susceptibility (right panel) in the VBS close to the phase boundary for $\mu/V = 11/12$, $t/V = 1/8$, and $T = t/24$. The BZ of the underlying triangular lattice is hexagonal (see Fig. 1), with corners at $\mathbf{Q} = (2\pi/3, 0)$ and symmetry related momenta. In both panels, the axes range from -2π to 2π , and ferromagnetic peaks at reciprocal lattice vectors have been suppressed.

suppresses the condensation of vortices and leads to a persistence of superfluidity [7].

At boson fillings $\rho = 1/3$ and $2/3$, the model in the large V/t limit can be mapped to a quantum dimer model on the hexagonal lattice, where the occupied (unoccupied) sites at $\rho = 1/3$ ($\rho = 2/3$) correspond to the presence of dimers. In the classical limit ($V/t = \infty$), all of the dimer coverings are degenerate. When V/t becomes large but finite, the degeneracy is partially lifted, and the remaining dimer kinetic energy promotes the so-called plaquette order [16,17]. In terms of bosons, for example, at $\rho = 2/3$, every third site on the kagome lattice forms a solid backbone of occupied sites, whereas the remaining bosons locally resonate around every third hexagon, as shown in Fig. 1. DVT at $\rho = 1/3$ and $2/3$ predicts several possible valence-bond order phases on the kagome lattice depending on the parameters of the effective field theory of the dual vortices. A set of mean-field states obtained by DVT are found to have the same spatial symmetry as the state described above. We expect that the kinetic energy gain would prefer the phase with the resonating hexagons. Our QMC data on $S(\mathbf{q})$ and $\chi(\mathbf{q})$ are consistent with these expectations; in particular, Bragg peaks are observed at the correct positions, as shown in Fig. 2. We find further QMC evidence for such resonances by measurements of the hexagon occupation. Denoting by P_n the measured fraction of hexagons with n bosons, we obtain $P_{0,1,2} < 10^{-3}$, $P_3 = 0.33(1)$, $P_4 = 0.38(2)$, $P_5 = 0.225(4)$, and $P_6 = 0.052(4)$ at various points inside the $\rho = 2/3$ solid, which compare well to the expected values P_n^e of $P_{0,1,2}^e = 0$, $P_3^e = 5/12$, $P_{4,5}^e = 1/4$, and $P_6^e = 1/12$ for the resonating state. Finally, we find sharp peaks in the bond structure factor and corresponding susceptibility at the corners of the kagome BZ. Figure 4 shows the finite-size scaling properties of the structure factor $S_b(\mathbf{q})/N = \langle B_{\mathbf{q}\tau} B_{\mathbf{q}\tau}^\dagger \rangle$ at $\mathbf{q} = \mathbf{Q}$, where $B_{\mathbf{q}\tau} = (1/N) \sum_\alpha B_{\alpha\tau} \exp(i\mathbf{q}\mathbf{r}_\alpha)$ summed over the bond index α connecting spins i and j ,

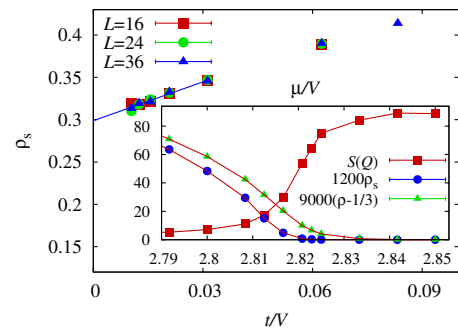


FIG. 3 (color online). The superfluid density ρ_s as a function of t/V at half filling for $\mu/V = 2$ and $T = t/5$. The lattice linear dimension is denoted L (see Fig. 1), so that the number of sites is $N = L \times L \times 3$. Inset: The static structure factor $S(\mathbf{Q})$, superfluid density ρ_s , and boson density ρ as a function of μ/V at $t/V = 1/10$, for $L = 24$ and $T = t/24$.

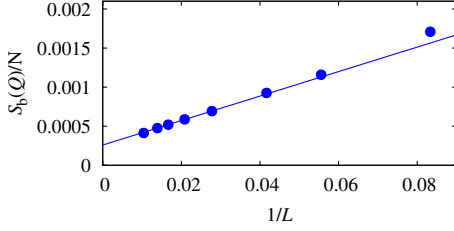


FIG. 4 (color online). Finite-size scaling of the bond structure factor $S_b(\mathbf{Q})$ in the VBS phase for $\mu/V = 11/12$, $t/V = 1/8$, and $T = t/12$. Error bars are smaller than the symbol sizes, and the line shows a linear extrapolation to the thermodynamic limit.

and $B_{\alpha(i,j),\tau} = t(b_i^\dagger b_j + b_i b_j^\dagger)_\tau$ is the off-diagonal bond operator at imaginary time τ . The nonzero intercept of the extrapolation in Fig. 4 exhibits long-range order in the bond-bond correlations [18]. The real-space correlations $C_b(\mathbf{r}_\gamma - \mathbf{r}_\delta) = \langle (\frac{1}{\beta} \int B_{\gamma\tau} d\tau - B_0) (\frac{1}{\beta} \int B_{\delta\tau} d\tau - B_0) \rangle$, where B_0 denotes the background bond strength, confirm the expected preponderance of resonating bonds on hexagons as illustrated in Fig. 5.

As shown in Fig. 2, “bow-tie” features appear in $S(\mathbf{q})$ and $\chi(\mathbf{q})$. At low temperatures and close to $\mathbf{q}_0 = (0, 2\pi/\sqrt{3})$ and equivalent positions, these can be fitted to $S(\mathbf{q}_0 + \mathbf{q}) \sim (q_\parallel^2 + \kappa^2)/\sqrt{q^2 + \kappa^2}$ and $\chi(\mathbf{q}_0 + \mathbf{q}) \sim (q_\parallel^2 + \kappa^2)/(q^2 + \kappa^2)$, where q_\parallel is a component of \mathbf{q} along the directions of bow ties, and κ is interpreted as an inverse correlation length. The bow ties are present in the solid phase and also in the superfluid phase near the transition, albeit with larger values of κ . Implications of this bow-tie structure will be discussed elsewhere [5].

In contrast to the case of a triangular lattice [13], we do not observe any obvious discontinuities that would indicate a first-order phase transition from the solid phases into the superfluid. An example is illustrated in Fig. 3, for ρ_s , $S(\mathbf{Q})$, and ρ along a cut at fixed t/V from the superfluid into the $\rho = 1/3$ solid. Landau-Ginzburg-Wilson (LGW) theory forbids a generic continuous transition between a solid and a superfluid, as different symmetries of H_b are broken in both phases. Possible explanations of our observation

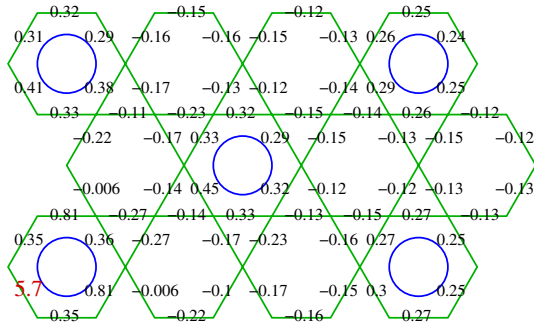


FIG. 5 (color online). The correlation function $C_b(\mathbf{r}_1 - \mathbf{r}_\delta)$ between the bond indicated by large (red) text and the other bonds for $L = 24$, $\mu/V = 11/12$, $t/V = 1/8$, and $T = t/12$.

would thus include (i) a *weakly* first-order superfluid-solid transition, at which the correlation length stays finite but exceeds the linear size of the QMC cells; (ii) a narrow intermediate supersolid regime; or (iii) a non-LGW continuous transition, such as the recently proposed deconfined quantum criticality scenarios [20,21]. To discern between these possibilities, we obtained detailed data and performed a finite-size scaling (FSS) study and analysis of energy histograms over the melting transition region.

We look first at the FSS behavior. For a two-dimensional system, the following FSS relations apply for a *continuous* solid to superfluid quantum phase transition. The superfluid density scales as $\rho_s = L^{-z} F_{\rho_s}(L^{1/\nu}(K_c - K), \beta/L^z)$, where L denotes the linear system size, z the dynamical critical exponent, ν the correlation length exponent, $K_c - K$ the distance to the critical point in terms of the control parameter K , such as t/V or μ/V , and F_{ρ_s} the corresponding scaling function. Similarly, $S(\mathbf{Q}) = L^{2-z-\eta} F_S(L^{1/\nu}(K_c - K), \beta/L^z)$ and $\chi(\mathbf{Q}) = L^{2-\eta} F_\chi(L^{1/\nu}(K_c - K), \beta/L^z)$, where η is the anomalous exponent. From these scaling relations, given appropriate values for $(t/V)_c$ and the critical exponents, QMC data for different system sizes should follow universal curves $F_{\rho_s}(\cdot, A)$ and $F_\chi(\cdot, A)$, if the transition is continuous.

QMC data were obtained over the melting transition, focusing on a fixed value of $\mu/V = 11/12$, which is close to the largest extend of the $\rho = 1/3$ solid. As discussed below, the scaling of the QMC data appears to be consistent with $z = 1$, so that most simulations were performed for fixed aspect ratios $A = \beta/L$. As shown in Fig. 6, the data for $\rho_s L$ appear to collapse very well for $(t/V)_c = 0.12821(2)$, $z = 1$, and $\nu = 0.43$. The data for $\chi(\mathbf{Q})$ also collapse well for $(t/V)_c = 0.12827(4)$, $\nu = 0.45$, and $\eta = -0.50(15)$. The two independent estimates for $(t/V)_c$ are sufficiently close in value to confirm a direct transition and make scenario (ii) seem unlikely. This is also consistent with the discovery of similar ν values on both sides of the transition. Based on the value of $\eta = -0.50(15)$, we also find the scaling of $S(\mathbf{Q})$ to be consistent with a dynamical exponent $z = 1.0(2)$.

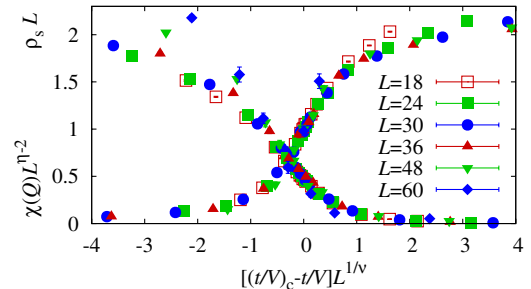


FIG. 6 (color online). Data collapse of the superfluid density ρ_s and static susceptibility $\chi(\mathbf{Q})$ at $\mu/V = 11/12$ for $\beta/L = 1/t$.

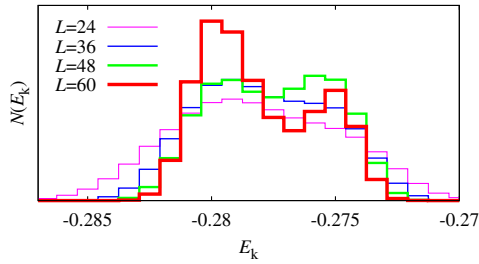


FIG. 7 (color online). Distribution (arbitrary units) of the kinetic energy close to the transition point for various system sizes, $\mu/V = 11/12$, $t/V = 1/7.796$, and $T = t/60$. As the system size increases, the double-peaked features become more pronounced.

Even though the FSS analysis appears to be consistent with a continuous quantum critical point in most respects, a negative value of η is unusual, and one may be inclined to interpret this as an indication of very *weak* first-order behavior. We explore this possibility in further detail by studying histograms of physical quantities in the transition region. In Fig. 7, one can see double-peaked structures developing in histograms of the kinetic energy over the melting transition for sufficiently large system sizes. We believe that this additional observation provides cogent evidence for scenario (i); i.e., the melting transition studied here is indeed very weakly first-order.

In conclusion, we have studied hard-core bosons on the kagome lattice with nearest-neighbor repulsion. At half filling, the model remains in a uniform superfluid phase for all values of V/t , and no supersolid emerges. For the solid phases at filling fractions $1/3$ and $2/3$, we find evidence for an exotic insulator with partially delocalized bosons occurring on a six-site hexagonal structure on the kagome lattice. Although the superfluid-solid melting transition appears naively to have the scaling properties of an unusual continuous quantum critical point, we find clear indication of weak first-order behavior from double-peaked histograms of the kinetic energy. The apparent weakness of this transition is in stark contrast to examples of strong first-order quantum melting transitions in related models [13]. An understanding of this contrasting behavior may have critical importance in the search for unconventional quantum criticality in this class of models and clearly deserves further study in the future.

This work was supported by the NSERC of Canada, CRC, CIAR (S. V. I. and Y. B. K.), as well as NIC Jülich and HLRS Stuttgart (S. W.). We thank R. Moessner, A. Paramekanti, A. Vishwanath, T. Senthil, A. Sandvik,

S. Sachdev, A. Honecker, K. Damle, N. Prokof'ev, and B. Svistunov for helpful discussions.

Note added.—Recently, we became aware of a parallel work [22] and thank its authors for correspondence.

-
- [1] R. Moessner and S. L. Sondhi, Phys. Rev. B **63**, 224401 (2001).
 - [2] L. Santos *et al.*, Phys. Rev. Lett. **93**, 030601 (2004); B. Damski *et al.*, Phys. Rev. A **72**, 053612 (2005).
 - [3] T. Matsubara and H. Matsuda, Prog. Theor. Phys. **16**, 569 (1956); **17**, 19 (1957).
 - [4] A. W. Sandvik, Phys. Rev. B **59**, R14 157 (1999); O. F. Syljuåsen and A. W. Sandvik, Phys. Rev. E **66**, 046701 (2002); K. Louis and C. Gros, Phys. Rev. B **70**, 100410 (2004).
 - [5] S. V. Isakov, S. Wessel, R. G. Melko, K. Sengupta, and Yong Baek Kim (unpublished).
 - [6] L. Balents *et al.*, Phys. Rev. B **71**, 144508 (2005).
 - [7] K. Sengupta, S. V. Isakov, and Yong Baek Kim, Phys. Rev. B **73**, 245103 (2006).
 - [8] G. Murthy, D. Arovas, and A. Auerbach, Phys. Rev. B **55**, 3104 (1997).
 - [9] K. Kano and S. Naya, Prog. Theor. Phys. **10**, 158 (1953).
 - [10] P. Nikolic and T. Senthil, Phys. Rev. B **71**, 024401 (2005); P. Nikolic, Phys. Rev. B **72**, 064423 (2005).
 - [11] E. L. Pollock and D. M. Ceperley, Phys. Rev. B **36**, 8343 (1987).
 - [12] D. Heidarian and K. Damle, Phys. Rev. Lett. **95**, 127206 (2005); R. G. Melko *et al.*, Phys. Rev. Lett. **95**, 127207 (2005).
 - [13] S. Wessel and M. Troyer, Phys. Rev. Lett. **95**, 127205 (2005).
 - [14] M. Boninsegni and N. Prokof'ev, Phys. Rev. Lett. **95**, 237204 (2005).
 - [15] J. Vidal *et al.*, Phys. Rev. B **64**, 155306 (2001).
 - [16] R. Moessner, S. L. Sondhi, and P. Chandra, Phys. Rev. B **64**, 144416 (2001).
 - [17] D. C. Cabra *et al.*, Phys. Rev. B **71**, 144420 (2005).
 - [18] The extrapolated value of order 10^{-4} appears to be quite small. However, the bond structure factor quantifies an off-diagonal correlation function, and order parameters constructed from such quantities typically are reduced in magnitude (from unity) due to quantum fluctuations. This value can be compared to the only other value available in the literature [19], where deep in the VBS phase the bond structure factor extrapolates to $\sim 10^{-3}$.
 - [19] A. W. Sandvik *et al.*, Phys. Rev. Lett. **89**, 247201 (2002).
 - [20] T. Senthil *et al.*, Science **303**, 1490 (2004); T. Senthil *et al.*, Phys. Rev. B **70**, 144407 (2004).
 - [21] E. Fradkin *et al.*, Phys. Rev. B **69**, 224415 (2004).
 - [22] K. Damle and T. Senthil, Phys. Rev. Lett. **97**, 067202 (2006).